Research article

Seung Ju Yoon, Da In Song, Jungmin Lee, Myung-Ki Kim, Yong-Hee Lee* and Chang-Kyu Kim*

Hopping of single nanoparticles trapped in a plasmonic double-well potential

https://doi.org/10.1515/nanoph-2020-0411
Received July 21, 2020; accepted September 28, 2020;
published online October 14, 2020

Abstract: Thermally induced particle hopping in the nanoscale double-well potential is fundamental in material design and device operation. After the proposal of the basic hopping theory, several experimental studies, including some using the optical trapping method, have validated the theoretical approach over various friction ranges of the surrounding medium. However, only external parameters, such as viscosity, temperature, and pressures, have been varied in practical circumstances, and other tools capable of adjusting the potential profile itself to modulate the hopping rate are needed. By using metallic nanoantenna with various gap sizes and different optical pump power, we engineered a double-well potential landscape and directly observed the hopping of a single nanoparticle with a diameter of 4 nm. The distance between the two potential wells was 0.6–5 nm, and the maximum well depth and maximum height of the central potential barrier were approximately 69 and 4 k_BT, respectively. The hopping rate was governed by the Arrhenius law and showed a vertex when the barrier height was approximately 2 k_BT, which was in good agreement with the computational expectations.

***Corresponding authors: Yong-Hee Lee**, Department of Physics, Korea Advanced Institute of Science and Technology (KAIST), Daejeon 34141, South Korea, E-mail: yhlee@kaist.ac.kr; and **Chang-Kyu Kim**, Department of Nano & Semiconductor Engineering, Korea Polytechnic University, Siheung 15073, South Korea,
E-mail: ckkim@kpu.ac.kr. https://orcid.org/0000-0003-4753-5320 (C.-K. Kim)
Seung Ju Yoon, Da In Song and Jungmin Lee, Department of Physics, Korea Advanced Institute of Science and Technology (KAIST), Daejeon 34141, South Korea, E-mail: smokyq@gmail.com (S.J. Yoon), fisdyne@kaist.ac.kr (D.I. Song), leejodu@gmail.com (J. Lee). https://orcid.org/0000-0001-7808-9031 (S.J. Yoon). https://orcid.org/0000-0001-8840-0428 (J. Lee)
Myung-Ki Kim, KU-KIST Graduate School of Converging Science and Technology, Korea University, Seoul 02841, South Korea,
E-mail: rokmk@korea.ac.kr. https://orcid.org/0000-0002-8896-6912

Keywords: Arrhenius factor; double-well potential; Kramers hopping; nanoantenna; plasmonics.

1 Introduction

The thermally driven hopping of a particle between two stable states over a potential barrier is a fundamental process in various phenomena such as thermal diffusion in solids [1–3], electron transport in semiconductors [4–6], adatom diffusion at crystal surfaces [7, 8], chemical reactions [9, 10], and folding dynamics in biomolecules [11–13]. Although Kramers provided a theoretical model for particle motion in a double-well potential in the 1940s, it was experimentally proved only recently because the manipulation and monitoring of nanoscale particles is challenging. The optical trapping method, in which an optically induced potential well captures a particle, has been widely used because it can handle a single particle noninvasively in a fluidic environment or vacuum, and it uses additional diagnostic schemes [14–17]. The fundamental way of controlling Kramers hopping is to change the properties of environmental material that transfers energy to a particle [3, 5, 7, 9–14], or the landscape of the potential well itself that constrains the particle [18–20]. In most cases, the external parameters such as temperature and pressure, which govern the viscosity of the surrounding medium, were adjusted to change the hopping characteristics of a particle [11–14]. Conversely, the hopping behavior when modulating the potentials has not been sufficiently investigated because of the difficulty in manipulating the energy level of an optical potential [21]. Another challenge is that in conventional optical platforms adopting a dielectric focusing lens, the size of the optical trap cannot be reduced beyond the diffraction limit of light; this restricts the diameter of particles available in the experiment to greater than tens of nanometers.

Plasmonic nanostructures, including double holes [22–24], nanodimers [25, 26], nanorods [27], and bow-tie antennas [28–32], have been developed to deal with smaller particles. A tightly confined electromagnetic field using surface plasmon polaritons can provide a nanometer-scale

potential well near the metal surface, and it can successfully demonstrate the trapping and releasing of a single nanoparticle. However, observing a transition inside a double-well optical potential is more crucial than the escape from an optical trap to fully understand the phenomenon and verify the Kramers theory. Furthermore, a systematic approach that can modify the potential profile is required.

In this work, we investigated the hopping of a single quantum dot (QD) trapped in an optical double-well potential formed by a metal nanoantenna with a bow-tie–shaped hole. The geometrical distance between the two apexes of the bow-tie nanoantenna and incident laser power changed both the lateral and vertical dimensions of the double-well potential. It provided a new framework to study the effect of the double-well potential on the particle hopping dynamics. A transmitted resonant pump laser (λ_ω = 1560 nm) and nonlinear second-harmonic (SH) signal ($\lambda_{2\omega}$ = 780 nm) confirmed the jump of a particle over the central potential barrier. The signal changes during the jumping were confirmed theoretically using finite-difference time-domain (FDTD) computations.

2 Results and discussion

2.1 Nanometer-scale optical double-well potential

A three-dimensional (3D) tapered metallic nanoantenna was used as a platform to build nanometer-sized optical traps (Figure 1A). Our bow-tie antenna formed in a 100-nm-thick Au layer on a 500-μm-thick SiO_2 substrate had a nanogap in the middle, and the detailed fabrication process is described in Supplementary material S1. The FDTD computations determined the electromagnetic energy distribution in the nanoantenna with the illumination of a 1560-nm wavelength laser, and a pair of tiny hot spots at the two vertices were detected (Figure 1B). Thus, a double-well potential profile was observed in the *yz*-plane. The antenna with a 5-nm gap has a mode volume of approximately $5 \times 5 \times 7$ nm^3 ($4.6 \times 10^{-8}\ \lambda^3$), which is six orders of magnitude smaller than the diffraction limit of light. The nanoscale mode volume enables the manipulation of a nanoparticle. Figure 1C shows the scanning electron microscopy images of the sample with a 5-, 7-, and 9-nm gap.

2.2 Tuning the optical potential landscape

The target substance was CdSe/ZnS QDs with a diameter of 4 nm and refractive index of 2.4. When the nanoantenna trapped a single QD, the electric field changed, and we obtained the resultant field distribution using FDTD simulation with Maxwell stress tensors (Supplementary material S2). Figure 2A shows the calculated optical potentials along the *y*-direction for a 10-mW continuous wave (CW) laser power. Here, the *y*-axis position represents the center-of-mass *y* coordinate of the QD as it moved along the slope. The two metal tips established a double-well potential profile along the *y*-direction, and a potential barrier existed between the two potential wells [33–35]. The difference in energy level between the top of the barrier and bottom of the well was an energy barrier height (U_b) for a QD. Furthermore, there were single potential wells along the *x*- and *z*-directions. However, we believe that the QD oscillations along these directions are rapid (ca. 3 MHz) [33, 36–38] that it is outside the measurement range (Supplementary material S3).

As the gap size between two metal tips decreased from 10 to 5 nm, the distance between the two potential wells shrunk, and the height of the central barrier decreased. Table 1 lists the numerical values of the distance between the double wells, depth of potential wells, and energy barrier height for various gap sizes. The pump power caused both the depth of potential wells and energy barrier height to increase linearly at –13 and 0.5 k_BT/10 mW, respectively (Supplementary material S2). Therefore, we could adjust the overall potential landscape by controlling the gap size and pump power. The oscillation frequencies at the bottom of the potential well (ω_0) and the top of the potential barrier (ω_b) were derived from the curvatures of the calculated potential energy profile (Table 1) [14, 16], and they increased linearly with the pump power. For the QD in the nanoantenna, there were two stable positions at the bottom of the two potential wells. Because the environmental medium, which was the water molecule in this experiment, transferred thermal energy to the trapped QD, it jumped between two stable states across the potential barrier. The parameters mentioned previously determined the theoretical hopping rate of QD using Equation S5 (Supplementary material S4).

The presence of QD in the metal gap changed the electric field distribution and resultant optical properties because of the dielectric filling effect. The transmittance was maximum when the QD was at the bottom of the potential well (empty red circles) and dropped as it passed through the barrier (filled red circle), as shown in Figure 2B. Moreover, the electric field intensity enhancement $|E|^2/|E_{\text{withoutQD}}|^2$, where E and $E_{\text{withoutQD}}$ are electric fields with and without a trapped QD, respectively, showed a peak when the QD was at the top of the potential barrier (filled blue circle) while it decreased as the QD moved back to the stable positions (empty blue circles). It induced a

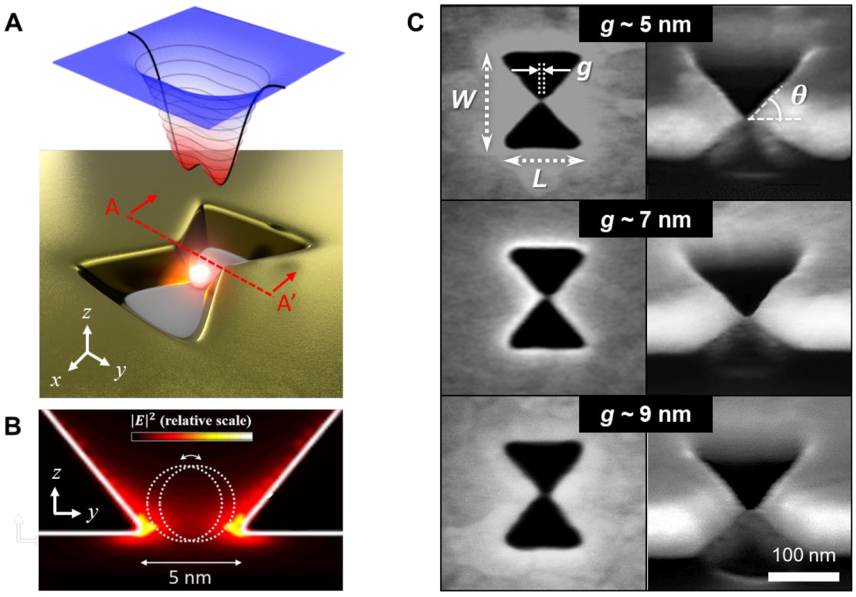

Figure 1: 3D plasmonic nanoantenna. (A) Schematic of particle trapping in the 3D antenna. Two focused lights inside the metal gap induced a double-well potential and enabled the trapping of a nanoparticle smaller than 5 nm. 3D surface graph represents the optical potential energy, and a black line is a cross-sectional profile in the *yz*-plane at the center of the nanoantenna. (B) $|E|^2$ distribution in the *yz*-plane along the line A-A′ when the 1560-nm wavelength *y*-polarized beam came from the bottom. Two stable positions of a nanoparticle (white dotted line) were depicted. The resonant mode of the nanoantenna was 1560 nm in water. (C) Scanning electron microscope images of the top and 52°-tilted views of the fabricated 3D plasmonic nanoantenna in the 100-nm-thick Au film on the glass substrate. The central gap size was measured to be approximately 5, 7, and 9 nm, respectively. The length, width, and vertical taper angle were 200 nm, 160 nm, and 65°, respectively.

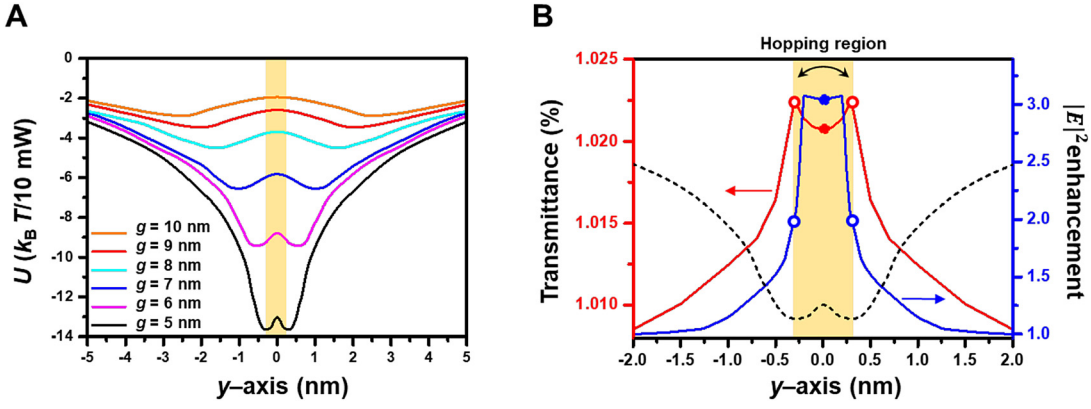

Figure 2: Double-well potential profile in 3D plasmonic nanoantenna. (A) Calculated optical potential energy (U) for a 4-nm-diameter QD moving along the *y*-axis for various metal gap sizes. Here, the incident CW laser power was 10 mW. The yellow area represents the hopping region of a nanoparticle in a 5-nm-gap nanoantenna. (B) Transmittance (red solid line) and electric field intensity enhancement (blue solid line) as a function of the QD position for a 5-nm-gap nanoantenna. A black dotted line is the potential profile.

Table 1: Calculated double-well potential properties with various gap sizes.

Gap size of the antenna (nm)	Distance between two wells (nm)	Depth of the potential at the antenna center (k_BT/10 mW)	Height of the central energy barrier U_b (k_BT/10 mW)	Oscillation frequency at the bottom of the well ω_0/10 mW (10^6 s^{-1})	Oscillation frequency at the top of the barrier ω_b/10 mW (10^6 s^{-1})
5	0.6	−13.0	0.50	284	71.2
6	1.2	−8.8	0.52	145	40.0
7	2.0	−5.8	0.58	22.4	17.8
8	3.0	−3.9	0.68	8.0	7.9
9	4.0	−2.6	0.75	2.6	4.8
10	5.0	−2.0	0.84	0.97	1.2

nonlinear effect on the metal surface so that the SH signal ($I_{2\omega}$) increased in proportion to the fourth power of an electric field (Supplementary material S6).

2.3 Experiments and roll-off frequency evaluation

Our trap-and-monitor system comprised two lasers: a 1560-nm CW laser for trapping QD and a femtosecond laser (100-fs pulses at 80 MHz) for SH generation (Supplementary material S5). The CW laser power (P_{CW}) was in the range of 10–70 mW (0.3–2.1 MW cm^{-2}). The average power of the femtosecond laser was 4.0 mW, and the peak power (12.5 GW cm^{-2}) was approximately 10,000 times greater than that of the CW laser. This two-laser platform provides the freedom to select the shape of the double-well potential as a function of the CW laser power and enables the measurement of additional information of background-free SH signal. We recorded both the transmission signal of pump lasers at λ_{ω} and SH pulses at $\lambda_{2\omega}$. When 2×10^{-6} M aqueous CdSe/ZnS QDs solution entered a microfluidic chamber, the metallic nanoantenna, which was placed in it, captured a single QD using an optical trap. The bandgap wavelength of the QDs was smaller than 780 nm, and the QDs were nonabsorptive at both the pump and SH wavelengths.

The sharp spikes in the transmission signal (I_{ω}) marked each hopping event of the QD between two stable states across the barrier of 5-nm-gap nanoantenna in Figure 3A. The simultaneously recorded SH pulses at $\lambda_{2\omega}$ also proved the QD hopping (Supplementary material S6). The series of spikes showed that the interval between hopping altered depending on P_{CW} (Figure 3B). For the quantitative analysis of hopping frequency, I_{ω} was transformed using a power spectral density method in Figure 3C. We fitted the power spectrum with a Lorentzian curve

$$S(f) = \frac{k_B T}{\pi^2 \beta \left(f_c^2 + f^2\right)} \tag{1}$$

where k_B is the Boltzmann constant, β is the Stokes' drag coefficient, T is the ambient temperature (300 K), and f_c is the roll-off frequency (or corner frequency) related to the trap stiffness α ($f_c = \alpha(2\pi\beta)^{-1}$).

The roll-off frequency was measured to increase from 3.0 Hz to the maximum value of 16 Hz until P_{CW} reached 40 mW. Interestingly, when P_{CW} increased further to 50 mW, the roll-off frequency reduced to 9 Hz. As P_{CW} increased, the potential well deepened and the oscillation frequency increased. This reduced the effective oscillation distance as well as the frictional energy loss during the hopping process. Therefore, the particle had a higher chance to oscillate

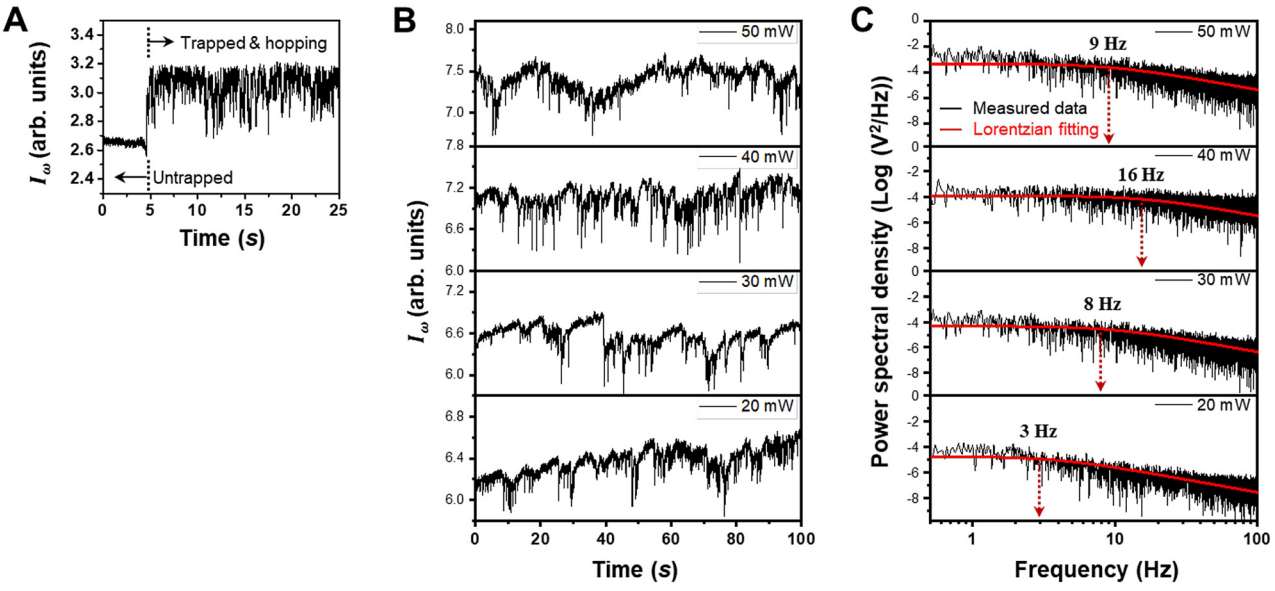

Figure 3: Modulation of quantum dot (QD) hopping rate with different input power.
(A) Transmitted signal intensity (I_{ω}) of incident lasers before and after the trapping of a 4-nm-diameter QD in a 5-nm-gap nanoantenna. A trapped QD increased the average transmittance, and each hopping event made a sharp spike. (B) Measured I_{ω} when the continuous wave (CW) laser power (P_{CW}) was 20, 30, 40, and 50 mW with the femtosecond laser power of 4 mW. (C) Power spectra of the measured signals (black dots) and Lorentzian fitting curves (red lines). When P_{CW} increased from 20 to 40 mW, the roll-off frequencies were measured to be 3, 8, and 16 Hz, respectively. When P_{CW} was 50 mW, the transition rate decreased to 9 Hz.

between two potential wells. By contrast, the rise of the potential barrier hindered the QD from crossing. These two effects competed with each other and maximized the hopping rates at specific pump laser powers.

This implies that the molecular thermal energy of the surrounding medium was the crucial factor that caused nanoparticle hopping in the double-well potential [1, 2, 18, 39]. In the low pump power range, the increase in the oscillation frequency promoted QD hopping as P_{CW} increased, whereas the low barrier did not considerably affect it. Because the barrier height increased at a rate of 0.5 k_BT/10 mW for the 5-nm-gap antenna, it became $2k_BT$ when P_{CW} was 40 mW. From this point, inhibition of QD hopping by the barrier was severely predominant because the thermal energy supplied by water molecules was at the level of k_BT [18, 39, 40]. The rate equation formula with the Arrhenius factor e^{-U_b/k_BT} (Equation S5) also supports the analytical interpretation of this turnover. In an overdamped regime like our experiment, the hopping rate is proportional to $\omega_0\omega_b\ e^{-U_b/k_BT}$, where ω_0, ω_b, and U_b linearly depend on P_{CW}. Therefore, the term is rewritten as $(U_b)^2e^{-U_b/k_BT}$ and has a maximum at $U_b = 2k_BT$ (Supplementary material S7). Samples with a broader gap revealed the same tendency.

2.4 Hopping characteristics of nanoantennas with various gap sizes

To facilitate the interpretation of the turnover phenomenon, we divided the nanoantennas into three groups by the gap size; group G1 corresponds to the gap size between 5 and 6 nm, group G2 between 7 and 8 nm, and group G3 between 9 and 10 nm. In Figure 4A–C, the hopping dynamics of all nanoantennas are plotted as a function of P_{CW}, and solid red lines represent the average of the measured transition rates at each power. In the experiment, the maximum limits of the pump power, indicated by vertical blue dotted lines, were set by the generation of air bubbles (Supplementary material S8). Because an increase

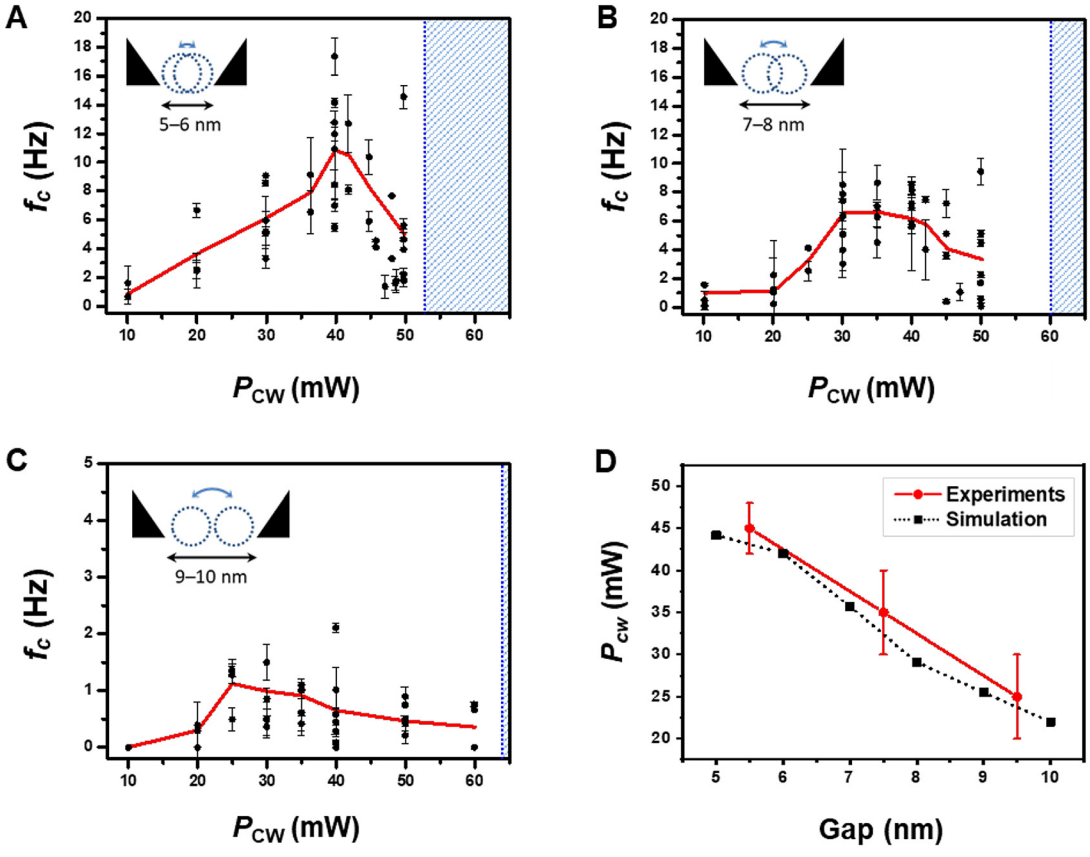

Figure 4: Measured roll-off frequencies in (A) group G1 (gap size of 5–6 nm), (B) group G2 (gap size of 7–8 nm), and (C) group G3 (gap size of 9–10 nm) as a function of the CW laser power (P_{CW}). The error bar represents the standard deviation of a Lorentzian fitting error. The solid red lines indicate the average of the roll-off frequencies at each P_{CW}. The vertical blue dotted lines at 53, 60, and 64 mW for group G1, G2, and G3, respectively, indicate the upper limit of P_{CW} due to air bubble generation. (D) Comparison of calculated and measured P_{CW} where the roll-off frequency has a vortex.

in the potential well depth was more significant than that of the thermal energy of water, the heat did not disrupt particle trapping in all measurements [23, 41]. By using the variation rate of the barrier height and water temperature as a function of P_{CW}, the computation predicted that maximum hopping rates were achieved when P_{CW} was in the range 42–44 mW for G1, 29–36 mW for G2, and 22–25 mW for G3, which had a U_b of approximately $2k_BT$. From the experiment, the maximum transition rates were obtained at P_{CW} of 40, 35, and 26 mW for G1, G2, and G3, respectively. These were in good agreement with the computational expectations, as depicted in Figure 4D.

3 Conclusions

In summary, we report the direct observation of a single QD hopping at the bottom of an optical double-well potential formed in a metallic nanogap antenna in water. By adjusting the gap size of the nanoantenna and the laser power, the distance between the two potential wells was 0.6–5 nm and the height of the central potential barrier could be increased to approximately $4k_BT$. A series of spikes in the pump laser's transmission signal showed the single hoppings of the QD over the barrier. From the different potential landscapes, we controlled the transition frequencies from 1 to 20 Hz. A turnover phenomenon that depended on the trapping power was observed for the hopping frequency. This was because of the competition between the potential barrier and the thermal energy of the surrounding medium. The effect of the Arrhenius factor becomes remarkable when the energy barrier approached $2k_BT$, and the measured turnover points agreed well with the theoretical prediction. The proposed platform provides a flexible way to control the potential landscape and to study the particle movements at the nanoscale. In addition, a control of the polarization direction or ellipticity of the trapping laser will enable more diverse potential profile implementations [41]. This will help in the understanding of phenomena related to nanoparticles such as chemical reactions near the surface, biomolecule dynamics in a vital inner vessel, and diffusion paths in multiplex potential systems on a solid surface.

Acknowledgments: C.-K. Kim acknowledges the support received from the National Research Foundation of Korea (NRF) grant funded by the Korea government (MSIT) (No. 2020R1F1A10482). M.-K. Kim acknowledges the support received from the KU-KIST School Project.

Author contribution: S.Y., C.K., M.K., and Y.L. conceived the idea and designed the experiments. S.Y. fabricated the samples, and S.Y., C.K., M.K., and Y.L. performed the experiments and analyzed the data. S.Y., D.S., and C.K. performed theoretical calculations. J.L. provided an in-depth discussion of the project. S.Y., C.K., and Y.L. wrote the manuscript.

Research funding: C.-K. Kim acknowledges the support received from the National Research Foundation of Korea (NRF) grant funded by the Korea government (MSIT) (No. 2020R1F1A10482). M.-K. Kim acknowledges the support received from the KU-KIST School Project.

Conflict of interest statement: The authors declare no conflicts of interest regarding this article.

References

[1] H. A. Kramers, "Brownian motion in a field of force and the diffusion model of chemical reactions," *Physica*, vol. 7, pp. 284–304, 1940.

[2] P. Hänggi, P. Talkner, and M. Borkovec, "Reaction-rate theory: fifty years after Kramers," *Rev. Mod. Phys.*, vol. 62, pp. 251–341, 1990.

[3] K. A. Velizhanin, S. Sahu, C. C. Chien, Y. Dubi, and M. Zwolak, "Crossover behavior of the thermal conductance and Kramers' transition rate theory," *Sci. Rep.*, vol. 5, p. 17506, 2015.

[4] S. Nettel, "Electron transport in semiconductors," *Phys. Rev. B*, vol. 30, pp. 1019–1020, 1984.

[5] P. Silvestrini, S. Pagano, R. Cristiano, O. Liengme, and K. E. Gray, "Effect of dissipation on thermal activation in an underdamped Josephson junction: first evidence of a transition between different damping regimes," *Phys. Rev. Lett.*, vol. 60, pp. 844–847, 1988.

[6] E. Turlot, D. Esteve, C. Urbina, et al., "Escape oscillations of a Josephson junction switching out of the zero-voltage state," *Phys. Rev. Lett.*, vol. 62, pp. 1788–1791, 1989.

[7] R. Guantes, J. L. Vega, S. Miret-Artés, and E. Pollak, "Kramers' turnover theory for diffusion of Na atoms on a Cu (001) surface measured by He scattering," *J. Chem. Phys.*, vol. 119, pp. 2780–2791, 2003.

[8] A. Alghannam, C. L. Muhich, and C. B. Musgrave, "Adatom surface diffusion of catalytic metals on the anatase TiO_2(101) surface," *Phys. Chem. Chem. Phys.*, vol. 19, pp. 4541–4552, 2017.

[9] G. O. Piloyan, I. D. Ryabchikov, and O. S. Novikova, "Determination of activation energies of chemical reactions by differential thermal analysis," *Nature*, vol. 212, p. 1229, 1966.

[10] A. M. Berezhkovskii, V. Y. Zitserman, S.-Y. Sheu, D.-Y. Yang, J. Kuo, and S. H. Lin, "Kramers theory of chemical reactions in a slowly adjusting environment," *J. Chem. Phys.*, vol. 107, pp. 10539–10554, 1997.

[11] M. Jacob, M. Geeves, G. Holtermann, and F. X. Schmid, "Diffusional barrier crossing in a two-state protein folding reaction," *Nat. Struct. Mol. Biol.*, vol. 6, pp. 923–926, 1999.

[12] R. B. Best and G. Hummer, "Diffusive model of protein folding dynamics with Kramers turnover in rate," *Phys. Rev. Lett.*, vol. 96, p. 228104, 2006.

[13] H. S. Chung and W. A. Eaton, "Single-molecule fluorescence probes dynamics of barrier crossing," *Nature*, vol. 502, pp. 685–688, 2013.
[14] L. Rondin, J. Gieseler, F. Ricci, R. Quidant, C. Dellago, and L. Novotny, "Direct measurement of Kramers turnover with a levitated nanoparticle," *Nat. Nanotechnol.*, vol. 12, pp. 1130–1133, 2017.
[15] A. Curran, M. P. Lee, M. J. Padgett, J. M. Cooper, and R. Di Leonardo, "Partial synchronization of stochastic oscillators through hydrodynamic coupling," *Phys. Rev. Lett.*, vol. 108, p. 240601, 2012.
[16] L. I. McCann, M. Dykman, and B. Golding, "Thermally activated transitions in a bistable three-dimensional optical trap," *Nature*, vol. 402, pp. 785–787, 1999.
[17] J. N. Wilking and T. G. Mason, "Multiple trapped states and angular Kramers hopping of complex dielectric shapes in a simple optical trap," *Europhys. Lett.*, vol. 81, p. 58005, 2008.
[18] G. Caratti, R. Ferrando, R. Spadacini, and G. E. Tommei, "Noise-activated diffusion in the egg-carton potential," *Phys. Rev. E*, vol. 54, pp. 4708–4721, 1996.
[19] A. Simon and A. Libchaber, "Escape and synchronization of a Brownian particle," *Phys. Rev. Lett.*, vol. 68, pp. 3375–3378, 1992.
[20] V. N. Smelyanskiy, M. I. Dykman, and B. Golding, "Time oscillations of escape rates in periodically driven systems," *Phys. Rev. Lett.*, vol. 82, pp. 3193–3197, 1999.
[21] Y. Seol, D. L. Stein, and K. Visscher, "Phase measurements of barrier crossings in a periodically modulated double-well potential," *Phys. Rev. Lett.*, vol. 103, p. 050601, 2009.
[22] Y. Pang and R. Gordon, "Optical trapping of 12 nm dielectric spheres using double-nanoholes in a gold film," *Nano Lett.*, vol. 11, pp. 3763–3767, 2011.
[23] Z. Xu, W. Song, and K. B. Crozier, "Direct particle tracking observation and Brownian dynamics simulations of a single nanoparticle optically trapped by a plasmonic nanoaperture," *ACS Photonics*, vol. 5, pp. 2850–2859, 2018.
[24] N. Hacohen, C. J. X. Ip, and R. Gordon, "Analysis of egg white protein composition with double nanohole optical tweezers," *ACS Omega*, vol. 3, pp. 5266–5272, 2018.
[25] B. J. Roxworthy, K. D. Ko, A. Kumar, et al., "Application of plasmonic bowtie nanoantenna arrays for optical trapping, stacking, and sorting," *Nano Lett.*, vol. 12, pp. 796–801, 2012.
[26] Z. Xu, W. Song, and K. B. Crozier, "Optical trapping of nanoparticles using all-silicon nanoantennas," *ACS Photonics*, vol. 5, pp. 4993–5001, 2018.
[27] W. Zhang, L. Huang, C. Santschi, and O. J. F. Martin, "Trapping and sensing 10 nm metal nanoparticles using plasmonic dipole antennas," *Nano Lett.*, vol. 10, pp. 1006–1011, 2010.
[28] J.-H. Kang, K. Kim, H.-S. Ee, et al., "Low-power nano-optical vortex trapping via plasmonic diabolo nanoantennas," *Nat. Commun.*, vol. 2, p. 582, 2011.
[29] P.-T. Lin, H.-Y. Chu, T.-W. Lu, and P.-T. Lee, "Trapping particles using waveguide-coupled gold bowtie plasmonic tweezers," *Lab Chip*, vol. 14, pp. 4647–4652, 2014.
[30] C. Pin, S. Ishida, G. Takahashi, K. Sudo, T. Fukaminato, and K. Sasaki, "Trapping and deposition of dye–molecule nanoparticles in the nanogap of a plasmonic antenna," *ACS Omega*, vol. 3, pp. 4878–4883, 2018.
[31] D. Verschueren, X. Shi and C. Dekker, "Nano-optical tweezing of single proteins in plasmonic nanopores," *Small Methods*, vol. 3, p. 1800465, 2020.
[32] S. J. Yoon, J. Lee, S. Han, et al., "Non-fluorescent nanoscopic monitoring of a single trapped nanoparticle via nonlinear point sources," *Nat. Commun.*, vol. 9, p. 2218, 2018.
[33] A. Zehtabi-Oskuie, H. Jiang, B. R. Cyr, D. W. Rennehan, A. A. Al-Balushi, and R. Gordon, "Double nanohole optical trapping: dynamics and protein-antibody co-trapping," *Lab Chip*, vol. 13, pp. 2563–2568, 2013.
[34] R. A. Jensen, I. C. Huang, O. Chen, et al., "Optical trapping and two-photon excitation of colloidal quantum dots using bowtie apertures," *ACS Photonics*, vol. 3, pp. 423–427, 2016.
[35] P. Mestres, J. Berthelot, S. S. Acimovic, and R. Quidant, "Unraveling the optomechanical nature of plasmonic trapping," *Light Sci. Appl.*, vol. 5, p. e16092, 2016.
[36] A. van der Horst and N. R. Forde, "Power spectral analysis for optical trap stiffness calibration from high-speed camera position detection with limited bandwidth," *Opt. Express*, vol. 18, pp. 7670–7677, 2010.
[37] R. Huang, I. Chavez, K. M. Taute, et al., "Direct observation of the full transition from ballistic to diffusive Brownian motion in a liquid," *Nat. Phys.*, vol. 7, pp. 576–580, 2011.
[38] R. Ferrando, R. Spadacini, G. E. Tommei, and G. Caratti, "Time scales and diffusion mechanisms in the Kramers equation with periodic potentials (I)," *Physica A*, vol. 195, pp. 506–532, 1993.
[39] J. L. Vega, R. Guantes, and S. Miret-Artés, "Mean first passage time and the Kramers turnover theory in activated atom–surface diffusion," *Phys. Chem. Chem. Phys.*, vol. 4, pp. 4985–4991, 2002.
[40] Q. Jiang, B. Rogez, J.-B. Claude, G. Baffou, and J. Wenger, "Temperature measurement in plasmonic nanoapertures used for optical trapping," *ACS Photonics*, vol. 6, pp. 1763–1773, 2019.
[41] L. Shao, D. Andrén, S. Jones, P. Johansson, and M. Käll, "Optically controlled stochastic jumps of individual gold nanorod rotary motors," *Phy. Rev. B*, vol. 98, p. 085404, 2018.

Supplementary Material: The online version of this article offers supplementary material (https://doi.org/10.1515/nanoph-2020-0411).